JMEPEG (2012) 21:1056–1060
DOI: 10.1007/s11665-011-9977-1
©ASM International
1059-9495/$19.00

Microstructures and Properties of Extruded Mg-Gd-Y-Zr Alloys Containing Zn

Hui-zhong Li, Hong-ting Liu, Fan-bo Li, Hai-jun Wang, Xiao-peng Liang, and Chu-ming Liu

(Submitted January 11, 2011; in revised form May 3, 2011)

Microstructure and mechanical properties of Mg-10Gd-3.8Y-*x*Zn-0.5Zr (*x* = 0, 1, 3 wt.%) alloys during extrusion and following isothermal aging at 200 °C were investigated using digital microhardness testing, mechanical testing, optical microscopy (OM), scanning electron microscopy (SEM), transmission electron microscopy (TEM), and x-ray diffraction (XRD). The results showed that Zn can refine grains of the alloy, and improved mechanical properties of the as-extruded alloys. In T5 (peak-aging) condition, the average grains of the alloy without Zn addition were about 20.10 μm; the average grains of the alloys with 1 wt.% Zn addition and 3 wt.% Zn addition were about 15.35 and 10.04 μm, respectively. For the alloy with 1 wt.% Zn addition in as-extruded and peak-aged states, the values of tensile strength reached 345 and 429 MPa, yield strength reached 260 and 342 MPa, as well as ductility rate reached 10.8 and 5.7%, respectively, exhibiting superior mechanical properties.

Keywords element Zn, extruded-aging, mechanical properties, Mg-10Gd-3.8Y-0.5Zr alloy, microstructure

1. Introduction

Mg-based alloys exhibit the notable advantages to the automotive and aerospace industries as structural parts due to their low densities and high strength per weight ratios. However, Mg alloys application has been limited to some components because of their low strength and poor heat resistance (Ref 1, 2). To the best of our knowledge, addition of rare-earth (RE) elements to the magnesium alloys improves the heat resistance and creep properties, e.g., WE54 commercial alloy (Ref 3). It has been confirmed that Gd element can obviously improve the strength of Mg alloys at elevated temperature because of the strengthening phase stability (Ref 4). In Mg-Gd alloys, high strengthening effect takes place during the decomposition of the solid solution with a kinetic character and with phase transformations that are in general the same as in the Mg-Y alloys (Ref 5). In addition, it has been reported that the Mg-Gd-Y alloy has a three-stage precipitation sequence: α-Mg (S.S.S.S.) → β″(DO_{19}) → β′(cbco) → β(fcc). Gao et al. (Ref 6) have demonstrated that the β′ precipitates grow to make the aging hardness increase rapidly, while β″ precipitates diminish and disappear. Moreover, the β′ phase is responsible for the peak hardness and is retained in both the peak-aged and over-aged structures (Ref 7).

Zn is often added for improving the mechanical properties by solid solution strengthening and age hardening (Ref 8, 9). Yamasaki et al. (Ref 10) have developed a hot-extruded Mg-2.3Zn-14Gd (wt.%) alloy which presents the highest tensile proof strength of 345 MPa and a better elongation of 6.3%, because of a coherent 14H long periodic stacking (LPS) structure precipitates from a supersaturated α-Mg matrix. It can be concluded that this phase has an effect on improving the mechanical properties of these alloys.

In this work, the microstructure and mechanical properties of Mg-10Gd-3.8Y-0.5Zr-*x*Zn (*x* = 0, 1, 3 wt.%) alloys during extrusion and following isothermal aging at 200 °C were investigated, in order to understand the effects of Zn addition on Mg-10Gd-3.8Y-0.5Zr alloy.

2. Experimental Procedure

The alloy ingots with nominal compositions shown in Table 1 were prepared from high purity Mg (>99.95%), Zn (>99.9%), and Mg-30.47%Gd, Mg-31.72%Y, Mg-31.16%Zr (wt.%) master alloys by melting in an electric resistance furnace at about 780 °C under the mixed atmosphere of CO_2 and SF6 with the ratio of 99:1. As-cast specimens 60 mm in diameter were homogenized at 520 °C for 12 h followed by quenching into water at 70-80 °C, and then they were hot extruded at 450 °C into rods of 17.2 mm in diameter and the extrusion ratio was 12.

The aging treatment was carried out at 200 °C with different times in an electric furnace. In this article, the aging treatment was carried out after extrusion immediately, and the T5 condition meant the peak-aging condition. In this condition, all the experimental alloys can gain better mechanical properties. Vicker hardness (HV) testing was taken using 4.9 N load and holding time of 15 s. The grain size was determined using a

Hui-zhong Li, Hong-ting Liu, Fan-bo Li, Hai-jun Wang, Xiao-peng Liang, and **Chu-ming Liu**, School of Materials Science and Engineering, Central South University, Changsha 410083, China; **Hui-zhong Li**, State Key Laboratory of Powder Metallurgy, Changsha 410083, China; and Key Laboratory of Nonferrous Metal Materials Science and Engineering, Ministry of Education, Central South University, Changsha 410083, China. Contact e-mail: hzli606@gmail.com.

linear intercept method from a large number of nonoverlapping measurements. The dimensions of the tensile specimens were 30 mm in gage length and 6 mm in gage diameter. Tensile testing was carried out on a uniaxial tensile testing machine at a crosshead speed of 2 mm/min. The tensile axis was aligned parallel to the extrusion direction.

Table 1 Chemical composition of test alloys

Alloy	Gd	Y	Zr	Zn	Mg
A	10	3.8	0.5	0	Bal.
B	10	3.8	0.5	1.0	Bal.
C	10	3.8	0.5	3.0	Bal.

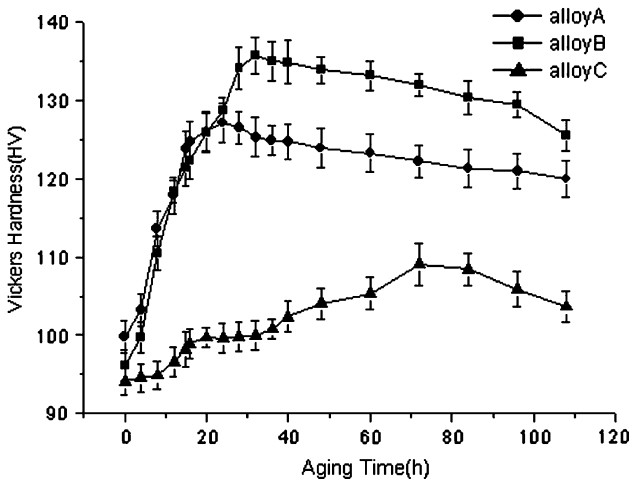

Fig. 1 Aging curves of the extruded samples at 200 °C

Table 2 Tensile properties of the alloys tested at room temperature

	Alloys	σ_b, MPa	$\sigma_{0.2}$, MPa	δ, %
Extruded	A	308	217	11.4
	B	345	260	10.8
	C	329	253	10.0
Extruded + T5 (200 °C)	A	401	296	6.9
	B	429	342	5.7
	C	415	327	5.0

Specimens for optical microscopy (OM) were prepared by a conventional mechanical polishing technique. The specimens were etched in 5 vol.% nitric acid alcohol solution. The microstructures of the samples were observed with Leica optical microscope. The precipitates morphology and the long-period stacking (LPS) structures of peak-aged specimens were observed by using a TEM (TecnaiG^{2}20) operated at an acceleration voltage of 200 kV. Thin foils for the TEM observations were prepared by twin jet electropolishing in a solution of 30% HNO_3 and 70% methanol cooled down to −30 °C, and then low energy beam ion thinning was carried out. Scanning electron microscope (Sirion200) and x-ray diffraction (D/MAX2500) were applied to carry out the phase analysis.

3. Results

3.1 Ageing Characteristics

Figure 1 shows the isothermal aging curves of A, B, and C alloys aged at 200 °C for different time intervals. The alloys of both A and B exhibit a rapid age-hardening respond at the initial stage of aging until they reach the peak hardness of 127 and 136 HV, which take time of 24 and 32 h, respectively, while the alloy C displays little aging hardening behaviors. Peak hardness value of alloy C is obtained at 72 h, with a peak hardness value of 109 HV. After that, the hardness of alloys A and B keep stable in a relatively long range and then drops gradually as a result of over-aging. However, the hardness of alloy C drops obviously after the peak value without any plateau of peak-aging region. It is suggested that adding suitable Zn to Mg-10Gd-3.8Y-0.5Zr-based alloy can greatly improve the age hardening responses. However, too much Zn addition (3 wt.%) will extend the peak-ageing time and decrease the peak hardness value.

3.2 Mechanical Properties

A comparison of the typical mechanical properties of all three alloys is listed in Table 2. In the as-extruded condition, the maximum ultimate tensile strength (UTS, σ_b) is obtained in alloy B, and the value is 345 MPa, it enhanced 37 MPa comparing with alloy A. The UTS of the alloys at room temperature (RT) increases with adding 1 wt.% Zn, and then decreases with further adding Zn (3 wt.%). The yield tensile strength (YTS, $\sigma_{0.2}$) of alloys at RT increases with 1 wt.% Zn addition, and the alloy C drops about 16 MPa than the alloy B. The elongations (δ) of the as-extruded specimens are high,

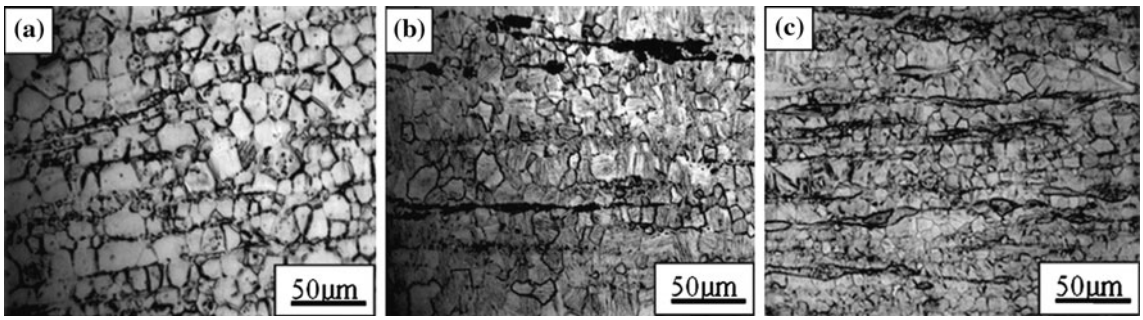

Fig. 2 OM images of the peak-aged samples (longitudinal direction): (a) alloy A, (b) alloy B, and (c) alloy C

especially the elongation of the alloy A, i.e., 11.4%. However, the elongation drops slightly with the additions of Zn, to 10.8 and 10.0% of the alloys B and C, respectively.

The mechanical properties of the specimens of these alloys peak aging at 200 °C are also improved compared with those of the alloy in as-extruded condition. Compared with the alloy A in as-extruded condition, the UTS is improved by 93 MPa, and the increment of YTS is 79 MPa, while the reduction of elongation is obviously, to 6.9%. The strengths of the peak-aging alloys tend to increase, while the elongations of these alloys are inclined to decrease with increasing the additions of Zn. The values of UTS and YTS of alloy B are 429 and 342 MPa, respectively, with an elongation of 5.7%. Further increasing the Zn content up to 3 wt.%, the tensile strength value of this alloy decreases rapidly, and the values of the UTS and YTS are 415 and 327 MPa, respectively. Meanwhile, the elongation of this alloy decreases, with a value of 5.0%. It is important to add suitable Zn to the Mg-Gd-Y-Zr-based alloys if we want to get superior mechanical properties.

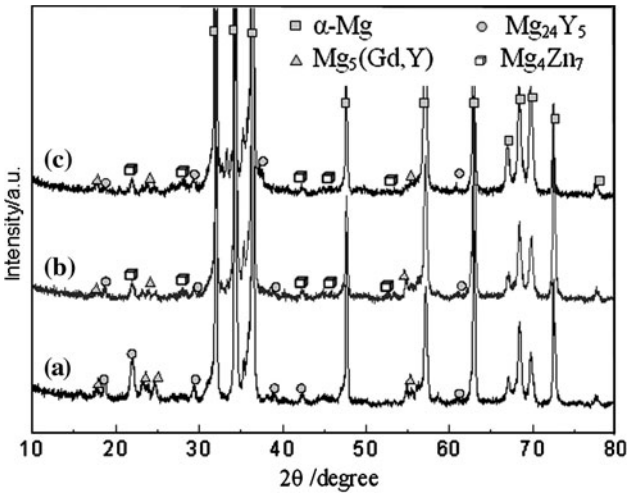

Fig. 3 X-ray diffraction pattern of peak-aged specimens: (a) alloy A, (b) alloy B, and (c) alloy C

3.3 Microstructures of the Peak-Aged Alloys

The optical micrographs of the peak-aged alloys are shown in Fig. 2. The average grain sizes of the alloys A, B, and C are round about 20.10, 15.35, and 10.04 μm, respectively. The grain sizes of these alloys decrease with increasing Zn content. It is suggested that the Zn addition has an obvious effect on refining the microstructure compared with the alloy A. It is concluded that the eutectic compounds with Zn have effect on limiting the growth of grains during extrusion.

Figure 3 shows the XRD patterns of the peak-aged specimens. The alloys are mainly composed of α-Mg solid solution, $Mg_{24}Y_5$, and $Mg_5(Gd,Y)$ secondary phases where Gd element probably substitutes for Y element. However, the phase constituents of alloys B and C is mainly composed of α-Mg solid solution, $Mg_{24}Y_5$, $Mg_5(Gd,Y)$, and Mg_4Zn_7 type phase.

Figure 4 shows the SEM images and energy dispersive x-ray spectra (EDS) microanalyses of compounds of the peak-aged specimens. The image at the higher magnification (Fig. 4c) shows that a lamellar phase appears with Zn addition

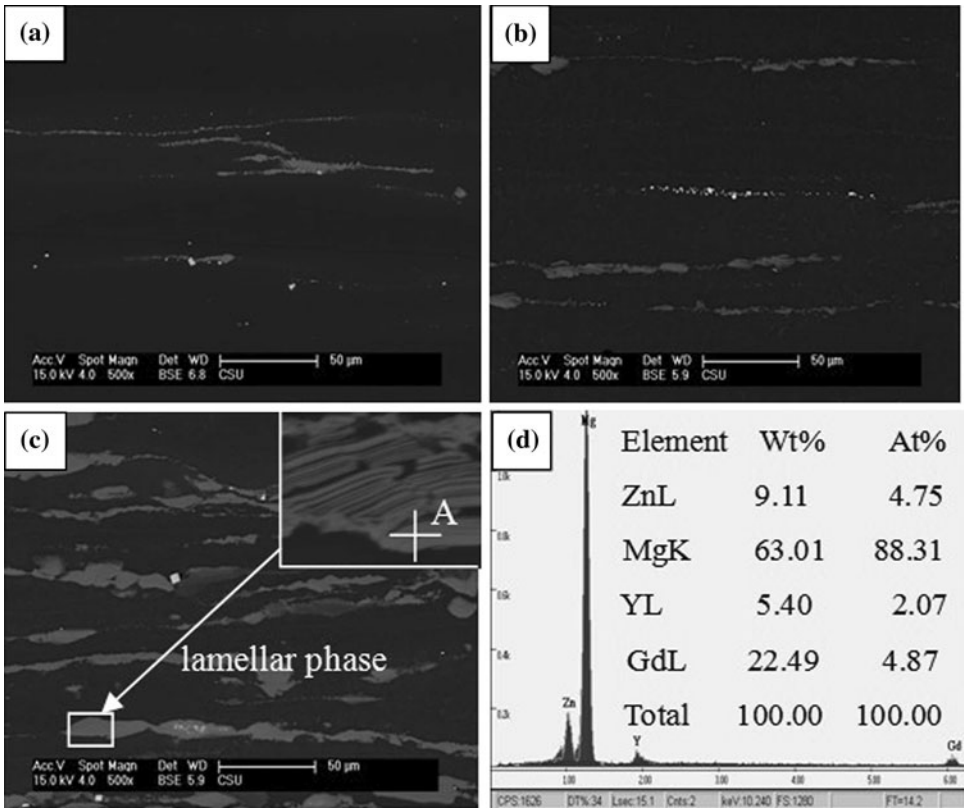

Fig. 4 SEM images and EDS microanalyse of compounds obtained from the peak-aged samples (longitudinal direction): (a) alloy A, (b) alloy B, (c) alloy C, and (d) corresponding EDS results of point A

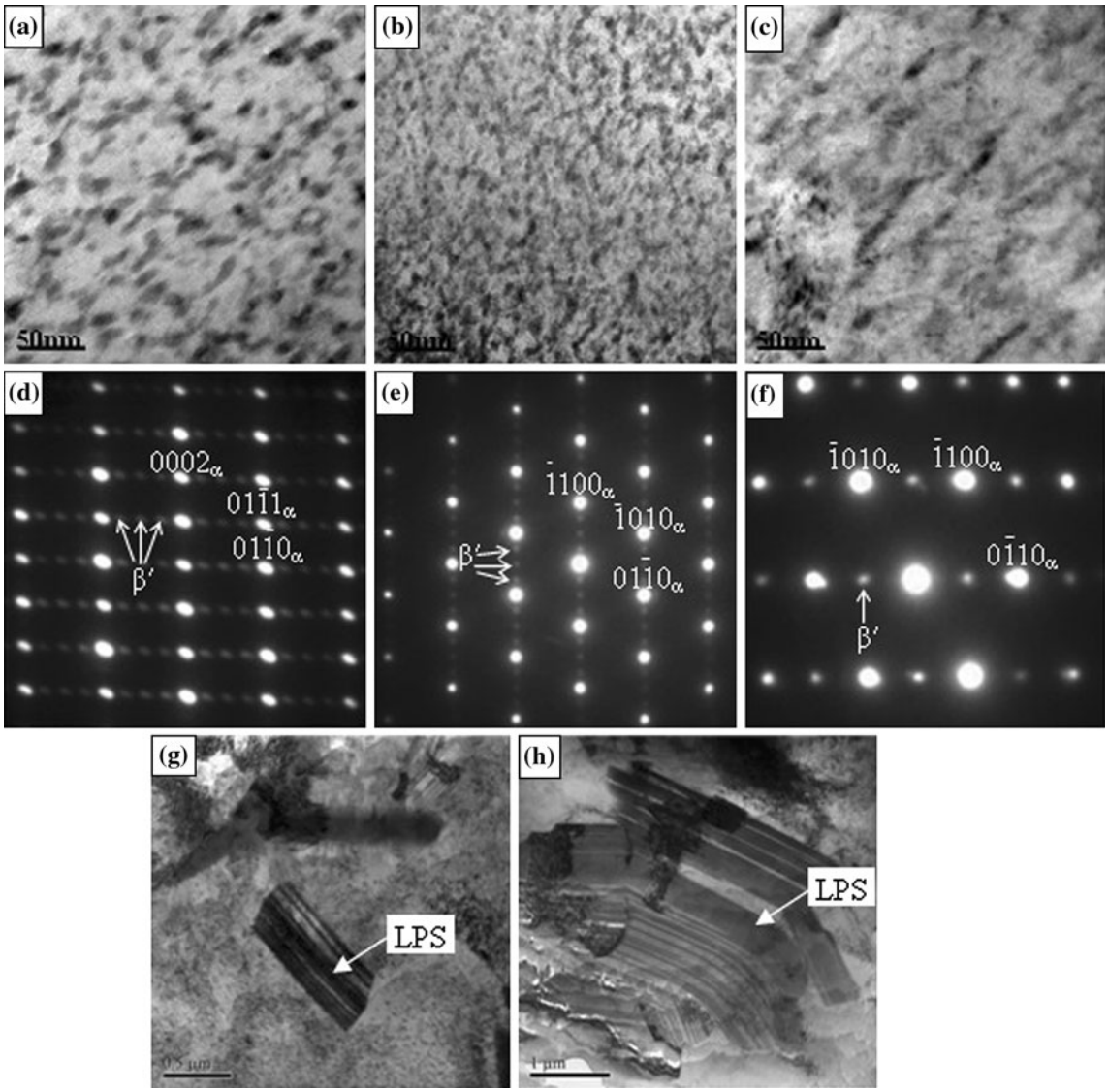

Fig. 5 TEM images and corresponding SAED patterns of specimens of the peak-aged alloys: (a) alloy A and corresponding SAED (d) $(B//[2\bar{1}\bar{1}0]_\alpha)$ patterns; (b) alloy B and corresponding SAED (e) $(B//[0001]_\alpha)$ patterns; (c) alloy C and corresponding SAED (f) $(B//[0001]_\alpha)$ patterns; (g) LPS structure of alloy B; (h) LPS structure of alloy C

and the volume fraction of this phase increases with increasing the content of Zn. Meanwhile, most of the intermetallic compounds have been destroyed and distribute along the extrusion direction.

In order to investigate the precipitation morphologies and discuss the reasons for the aging response at 200 °C, the TEM images and corresponding SAED patterns from the peak-aged alloys are shown in Fig. 5. The precipitates are identified by SAED, to be β′ phase, shown in Fig. 5(d), (e), and (f). Figure 5(a) shows that a great number of β′ particles which are ellipsoidal in morphology are observed in the peak-aged specimens of alloy A. These particles are distributed throughout the matrix, and the average size of this phase is smaller while the volume fraction is higher in the peak-aged specimens of alloy B, shown in Fig. 5(b). However, the average size of these particles in alloy C is bigger and lower density number than that in alloy A. It is suggested that too much Zn addition will coarsen this β′ phase.

The other the precipitation in Zn addition alloy is the LPS structure in a lamellar morphology, as seen in Fig. 5(g) and (h). The average size of these LPS structures in alloy B is about 0.8 μm in length and 0.4 μm in thickness. However, the average size of these LPS structures in alloy C is bigger than that in alloy B, with a longness of 4.5 μm and a thickness of 3 μm. It is suggested that the average size of these structures increases with increasing Zn addition.

4. Discussion

It is the commercial interesting to explore the high strength magnesium alloys by adding low-cost elements, such as Zn. Obviously, greater aging hardening responses and significantly higher tensile strength values are obtained in 1% Zn addition alloy. The average grain sizes of the alloys A, B, and C are

round about 20.10, 15.35, and 10.04 μm, respectively. It is confirmed that improvement of the mechanical properties is mostly attributed to microstructure refinement. In previous studies, it was shown that plastic deformation processes such as extrusion of Mg alloys with LPS structures are effective in strengthening the alloys, because the extrusion process brings about refining of α-Mg grains and also substantial dispersion of the hard lamellar phase, LPS structures (Ref 11-13). The Mg alloys containing the LPS structure are promising materials for wrought Mg alloys. The extrusion process brings about moderate and continuous bending of the LPS structure by any given angle (Fig. 5h). The high strength seems to originate in the highly dispersed and bent LPS structures as well as the refinement of α-Mg matrix grains. As shown in Table 2, the tensile strength of extruded alloy B and alloy C with LPS structures are higher than that of the as-extruded alloy without LPS structures. The average size of these LPS structures in alloy C is much bigger than that in alloy B, which becomes the cores of a fracture, leading to lower UTS value.

Suzuki et al. suggested that the strengthening effects of Zn might be due to decrease in stacking fault energy and consequent reduction of mobility of dislocations (Ref 14). Nie et al. also reported that enhanced strength in the Mg-6Gd-1Zn-0.6Zr alloy resulted from a uniform and dense distribution of basal precipitate plates (Ref 15), particularly β′ and β″ phases even β1 phase (Ref 16-18). Alloy A has high volume fraction of β′ phase as a result of a great increase in tensile strength in the peak-aged condition. The average size of β′ phase is smaller while the volume fraction is higher in the peak-aged specimens of alloy B, shown in Fig. 5(b). The strengthening contribution from this smaller phase is about 28 MPa higher than that of alloy A. However, because of coarsening of these precipitates, the strength value of alloy C decreases to 415 MPa, 14 MPa less than that of alloy B.

Besides, with the addition of 1 wt.% Zn to Mg-10Gd-3.8Y-0.5Zr-based alloy, there will occur more β′ phases and the LPS structures. However, with more Zn addition, up to 3 wt.%, it will form more larger LPS structures, shown in Fig. 5(h). To form these LPS structures, which contain Gd, Y, and Zn (Fig. 4d), it needs more RE (standing for Gd and Y) from the α-matrix. As a result, the content of RE retained in the supersaturated solution of the matrix decreased. The more Zn is added, the less RE is left in the matrix. Hence, when these alloys were aged, the decrement of the RE concentration leads to little age hardening response and prolong the time to peak-aged of these Mg-Gd-Y-Zr-based alloys which contain higher Zn, i.e., alloy C.

5. Conclusions

The microstructures and the tensile properties of alloys A, B, and C have been investigated by an OM, XRD, SEM, and TEM in this article. The investigation can lead to the following conclusions:

1. The result shows that the Zn addition has reduced the grain sizes. The LPS structure has been observed in the as-extruded alloys that contain Zn. The improvement of the tensile strength of the as-extruded alloys B and C is mainly ascribed to the presence of LPS structure and the smaller grain sizes. The values of the UTS and YTS of alloy B are 345 and 260 MPa at RT, respectively.
2. Addition of 1% Zn to Mg-10Gd-3.8Y-0.5Zr alloy brings a greater magnitude aging response and longer time to reach peak hardness. The peak-aged alloy B exhibits the highest peak hardness and tensile strength, and the values of the UTS and YTS are 429 and 342 MPa, respectively. It was due to the β′ phase that precipitated within the matrix during aging at 200 °C.

References

1. S.Y. Xu, S.Y. Long, and F.G. Li, A Novel Squeeze Casting Process for Producing Magnesium Wheels, Mater, *Sci. Forum*, 2007, **546–549**, p 113–118
2. B.L. Mordike and T. Ebert, Magnesium Properties-Application-Potential, *Mater. Sci. Eng. A*, 2001, **302**(1), p 37–45
3. I.J. Polmear, Magnesium Alloys and Applications, *Mater. Sci. Technol.*, 1994, **10**(1), p 1–16
4. I. Stulíková, B. Smola, Buch Fvon, and B.L. Mordike, Mechanical Properties and Creep of Mg-Rare Earth-Sc-Mn Squeeze Cast Alloys, *Materialwiss. Werkstofftech.*, 2003, **34**(1), p 102–108
5. L.L. Rokhlin and I.N. Nikitina, Magnesium-Gadolinium and Magnesium-Gadolinium-Yttrium Alloys, *Z. Metallkunde*, 1994, **85**(12), p 819–823
6. X. Gao, S.M. He, X.Q. Zeng, L.M. Peng, W.J. Ding, and J.F. Nie, Microstructure Evolution in a Mg-15Gd-0.5Zr (wt.%) Alloy During Isothermal Aging at 250°C, *Mater. Sci. Eng. A*, 2006, **431**(1–2), p 322–327
7. C. Antion, P. Donnadieu, F. Perrard, A. Deschamps, C. Tassin, and A. Pisch, Hardening Precipitation in a Mg-4Y-3RE Alloy, *Acta Mater.*, 2003, **51**(18), p 5335–5348
8. L.Y. Wei, G.L. Dunlop, and H. Westengen, Precipitation Hardening of Mg-Zn and Mg-Zn-RE Alloys, *Metall. Mater. Trans. A*, 1995, **26**(7), p 1705–1716
9. M. Suzuki, T. Kimura, J. Koike, and K. Maruyama, Strengthening Effect of Zn in Heat Resistant Mg-Y-Zn Solid Solution Alloys, *Scr. Mater.*, 2003, **48**(8), p 997–1002
10. M. Yamasaki, T. Anan, S. Yoshimoto, and Y. Kawamura, Mechanical Properties of Warm-Extruded Mg-Zn-Gd Alloy With Coherent 14H Long Periodic Stacking Ordered Structure Precipitate, *Scr. Mater.*, 2005, **53**(7), p 799–803
11. E. Abe, Y. Kawamura, K. Hayashi, and A. Inoue, Long-Period Ordered Structure in a High-Strength Nanocrystalline Mg-1 at% Zn-2 at% Y Alloy Studied by Atomic-Resolution Z-Contrast STEM, *Acta Mater.*, 2002, **50**(15), p 3845–3857
12. S. Yoshimoto, M. Yamasaki, and Y. Kawamura, Microstructure and Mechanical Properties of Extruded Mg-Zn-Y Alloys with 14H Long Period Ordered Structure, *Mater. Trans.*, 2006, **47**(4), p 959–965
13. Y. Kawamura and M. Yamasaki, Formation and Mechanical Properties of $Mg_{97}Zn_1RE_2$ Alloys with Long-Period Stacking Ordered Structure, *Mater. Trans.*, 2007, **48**(11), p 2986–2992
14. M. Suzuki, T. Kimura, J. Koike, and K. Maruyama, Effects of Zinc on Creep Strength and Deformation Substructures in Mg-Y Alloy, *Mater. Sci. Eng. A*, 2004, **387–389**, p 706–709
15. J.F. Nie, X. Gao, and S.M. Zhu, Enhanced Age Hardening Response and Creep Resistance of Mg-Gd Alloys Containing Zn, *Scr. Mater.*, 2005, **53**, p 1049–1053
16. I.A. Anyanwu, S. Kamado, and Y. Kojima, Aging Characteristics and High Temperature Tensile Properties of Mg-Gd-Y-Zr Alloys, *Mater. Trans.*, 2001, **42**(7), p 1206–1211
17. I.A. Anyanwu, S. Kamado, and Y. Kojima, Creep Properties of Mg-Gd-Y-Zr Alloys, *Mater. Trans.*, 2001, **42**(7), p 1212–1218
18. T. Kawabata, K. Matsuda, S. Kamado, Y. Kojima, and S. Ikeno, HRTEM Observation of the Precipitates in Mg-Gd-Y-Zr Alloy, *Mater. Sci. Forum*, 2003, **303**, p 419–422